Coupling of Trade Winds with Ocean Circulation Damps ITCZ Shifts

BRIAN GREEN AND JOHN MARSHALL

Department of Earth, Atmospheric, and Planetary Sciences, Massachusetts Institute of Technology, Cambridge, Massachusetts

ABSTRACT

The position of the intertropical convergence zone (ITCZ) is sensitive to the atmosphere's hemispheric energy balance, lying in the hemisphere most strongly heated by radiative and turbulent surface energy fluxes. This study examines how the ocean circulation, through its cross-equatorial energy transport and associated surface energy fluxes, affects the ITCZ's response to an imposed interhemispheric heating contrast in a coupled atmosphere–ocean general circulation model. Shifts of the ITCZ are strongly damped owing to a robust coupling between the atmosphere's Hadley cells and the ocean's subtropical cells by the trade winds and their associated surface stresses. An anomalous oceanic wind-driven cross-equatorial cell transports energy across the equator, strongly offsetting the imposed heating contrast. The circulation of this cell can be described by the combination of trade wind anomalies and the meridional gradient of sea surface temperature, which sets the temperature contrast between its upper and lower branches. The ability of the wind-driven ocean circulation to damp ITCZ shifts represents a previously unappreciated constraint on the atmosphere's energy budget and indicates that the position of the ITCZ may be much less sensitive to interhemispheric heating contrasts than previously thought. Climatic implications of this damping are discussed.

1. Introduction and background

Tropical rainfall is often organized into east–west bands, which collectively are referred to as the intertropical convergence zone. The global ITCZ moves between the Northern and Southern Hemispheres (NH and SH) over the seasonal cycle, following the sun's heating, and resides in the NH in the annual mean (Donohoe et al. 2013). Large-scale vertical motion in the tropical atmosphere is collocated with the ITCZ, where moist convection reduces the stratification experienced by those flows (Emanuel et al. 1994; Neelin 1997). Consequently, the ITCZ covaries with the ascending branch of the Hadley circulation, whose two cells are closed by descent in the subtropics and are shown schematically in Fig. 1. These two thermally direct cells transport energy in the direction of their upper branches, poleward and away from the ITCZ. The ITCZ's position is then anticorrelated with the atmosphere's

cross-equatorial energy transport and lies in the hemisphere from which the Hadley circulation transports energy in the long-term mean (Marshall et al. 2014; Frierson et al. 2013), over the seasonal cycle (Donohoe et al. 2013), and in interannual variability (Donohoe et al. 2014; Adam et al. 2016).

The relationship between the ITCZ position and atmospheric cross-equatorial energy transport is shown schematically in Fig. 1. When the ITCZ and Hadley cells are biased north of the equator (Fig. 1a), the total Hadley circulation can be thought of as a superposition of hemispherically symmetric (Fig. 1b) and asymmetric components (Fig. 1c). At a given latitude ϕ, this decomposition of the total meridional overturning streamfunction ψ is expressed as follows:

$$\psi(\phi) = \psi_{\text{Sym}}(\phi) + \psi_{\text{Asym}}(\phi), \tag{1a}$$

$$\psi_{\text{Sym}}(\phi) = \frac{1}{2}[\psi(\phi) - \psi(-\phi)], \quad \text{and} \tag{1b}$$

$$\psi_{\text{Asym}}(\phi) = \frac{1}{2}[\psi(\phi) + \psi(-\phi)]. \tag{1c}$$

Because the symmetric Hadley cells cannot transport mass and energy across the equator, the asymmetric cells are entirely responsible for the cross-equatorial

---

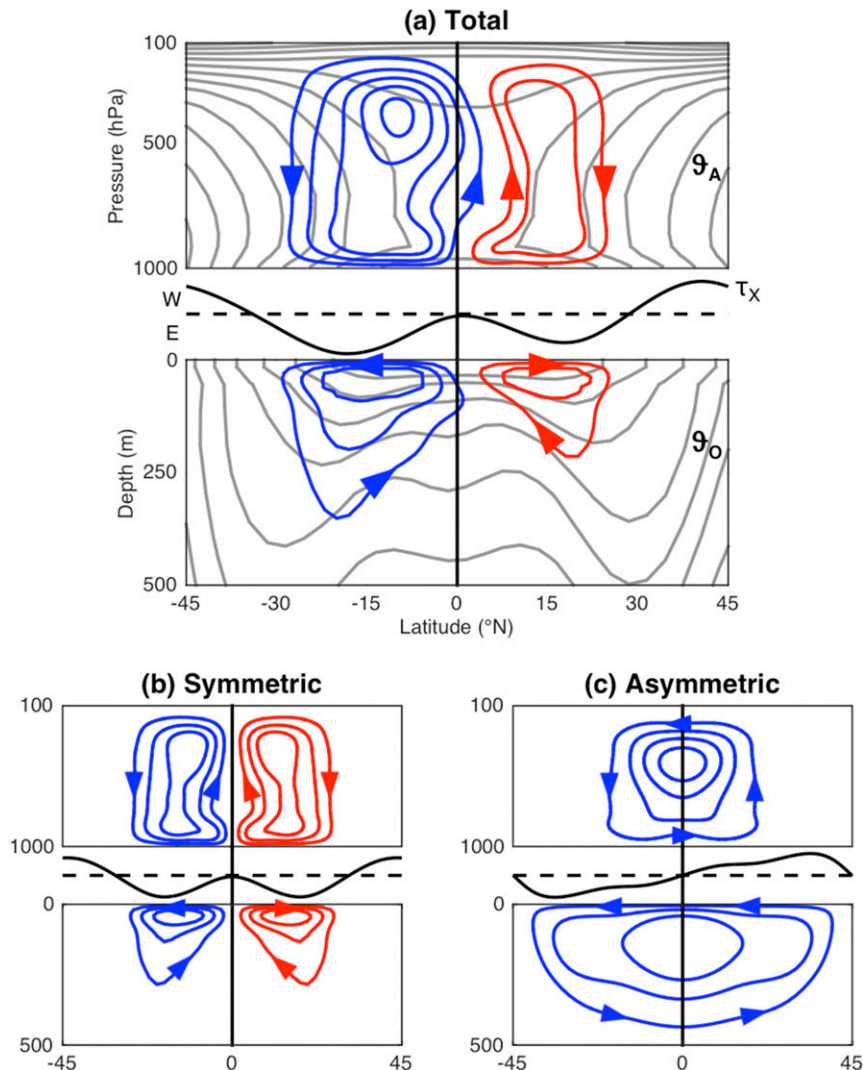*Corresponding author e-mail*: Brian Green, brianmg@mit.edu

FIG. 1. Schematic of the atmosphere–ocean circulation. (a) The (top) total atmosphere circulation, (middle) surface zonal wind stress on the ocean (E indicates easterly and W indicates westerly), and (bottom) ocean circulation. Contours of moist static energy ϑ_A and water temperature ϑ_O are shown in gray, generally increasing in value upward and equatorward. (b) As in (a), but for the symmetric component of the atmosphere and ocean circulations and the surface zonal wind stress. (c) As in (a), but for the asymmetric component of the atmosphere and ocean circulations and the surface zonal wind stress.

energy transport. With rising air in the NH and descent closing the circulation in the SH, the asymmetric cell rotates counterclockwise for an ITCZ residing in the NH; it rotates in the opposite sense if the ITCZ is in the SH. Combined with a positive stratification (gray lines in Fig. 1a), the asymmetric Hadley cell transports energy southward across the equator away from the ITCZ.

A corollary of the connection between the ITCZ's position and cross-equatorial energy transport by the atmosphere is that the ITCZ is sensitive to the atmosphere's hemispheric energy balance. Heating of one hemisphere's atmosphere relative to the other affects the ITCZ's

position by inducing the atmosphere to transport a fraction of the heating imbalance across the equator, a process sometimes referred to as "compensation" (Kang et al. 2008). As a result, the ITCZ resides in the hemisphere heated most strongly by the combination of radiative fluxes at the surface and top of atmosphere and surface fluxes of sensible and latent heat. Its position can then be affected by a variety of factors not necessarily confined to the tropics and is sensitive to any hemispherically asymmetric forcing [see the review in Schneider et al. (2014)].

Within this energy balance framework, several modeling studies have sought to understand the ITCZ's

response to a variety of forcings and feedbacks. For example, if an anomalous freshwater flux is added to the North Atlantic, the ITCZ shifts southward as a slow-down in the Atlantic's meridional overturning circulation (AMOC) fluxes less energy across the equator and into the extratropical NH atmosphere (Zhang and Delworth 2005; Broccoli et al. 2006). Increases in NH high-latitude ice cover, via their impact on surface albedo, can cool the atmosphere and result in a southward ITCZ shift away from the cooling (Chiang and Bitz 2005; Broccoli et al. 2006). Clouds have a strong impact on Earth's energy budget, and hemispheric asymmetries in their distribution can lead to ITCZ biases in climate models (Hwang and Frierson 2013) and can affect the magnitude of the ITCZ's response to interhemispheric albedo contrasts (Voigt et al. 2014).

The focus of the above studies has been on the atmosphere's ability to compensate an interhemispheric heating contrast by shifting the ITCZ and transporting energy across the equator. Compared to the ocean, though, the atmosphere is inefficient at transporting energy in the tropics, where moist convection and the weak effects of rotation lead to weak moist static energy gradients away from the surface (Charney 1963; Neelin and Held 1987; Czaja and Marshall 2006). Thus, the Hadley cells in the deep tropics cannot act on large energy gradients to transport energy. In contrast, the tropical ocean is strongly stratified in temperature, and the wind-driven subtropical cells (STCs; McCreary and Lu 1994) efficiently transport energy away from the equator owing to the surface temperature difference between the tropics and subtropics (Klinger and Marotzke 2000; Held 2001; Czaja and Marshall 2006). Even though the STCs transport less mass than the Hadley cells, the ocean circulation is estimated to cool the tropics more strongly than the atmosphere in the annual mean (Trenberth and Caron 2001).

The STCs, because they are driven by trade winds imparting a surface stress, are strongly coupled to shifts in the Hadley circulation and the ITCZ. A northward shift of the ITCZ is accompanied by a weakening of the easterly wind stress in the NH and an enhancement in the SH (Lindzen and Hou 1988). This asymmetric pattern drives southward Ekman flow in the ocean in both hemispheres. If this warm southward surface flow crosses the equator and is returned at depth at cooler temperatures, a southward cross-equatorial energy transport would result, which cools the NH. This NH cooling would push the ITCZ southward, damping the initial northward shift. Hemispherically asymmetric wind stress patterns drive cross-equatorial near-surface flow and energy transports in, for example, the Indian Ocean in the annual

mean (Miyama et al. 2003) and the global ocean over the seasonal cycle (Jayne and Marotzke 2001).

Here we explore the role of the ocean circulation and its cross-equatorial energy transport in damping ITCZ shifts in response to a heating of one hemisphere relative to the other. We find that cross-equatorial energy transport by the ocean is able to strongly compensate the imposed interhemispheric heating contrast, damping an ITCZ shift by a factor of 4 compared to the case where the ocean circulation is not allowed to respond to the forcing. The Hadley cells and STCs accomplish the majority of the cross-equatorial energy transport in the atmosphere and ocean, and their respective strengths are coupled by the surface wind stress associated with the trade winds. Similar to the atmosphere in Fig. 1, the ocean circulation and surface wind stress distribution can be decomposed into symmetric and asymmetric components, with the asymmetric component of the ocean circulation responsible for its cross-equatorial energy transport. We will show that the asymmetric atmosphere and ocean circulations are coupled by the asymmetric trade wind stress distribution and are thus constrained to overturn in the same sense. Furthermore, because their upper branches have higher energy densities than their lower branches, the Hadley cells and STCs will always transport energy in the same direction, damping ITCZ shifts compared to the atmosphere-only case.

Coupling of the Hadley cells and the STCs by the surface wind stress distribution, along with the resulting implications for meridional energy transport, has been discussed for a hemispherically symmetric atmosphere by Held (2001) and Czaja and Marshall (2006). However, the coupling of the asymmetric circulations, their cross-equatorial energy transport, and the implications for ITCZ shifts have only been speculated on in passing in box 1 of Schneider et al. (2014). Recent studies with coupled ocean–atmosphere GCMs note that the ocean and its cross-equatorial energy transport can damp ITCZ shifts in response to changes in Southern Ocean cloud properties (Kay et al. 2016; Hawcroft et al. 2016; Mechoso et al. 2016) and Arctic sea ice concentrations (Tomas et al. 2016), but the mechanisms responsible for this damping remain unclear. Our results and analysis propose that a wind-driven hemispherically asymmetric ocean circulation might be responsible for the damped ITCZ shifts in these studies.

Our paper is set out as follows. In section 2, we describe experiments in which a coupled atmosphere–ocean general circulation model (GCM) is forced by an interhemispheric albedo contrast. The model is run both with and without an active ocean circulation to highlight the role of the ocean's circulation in the
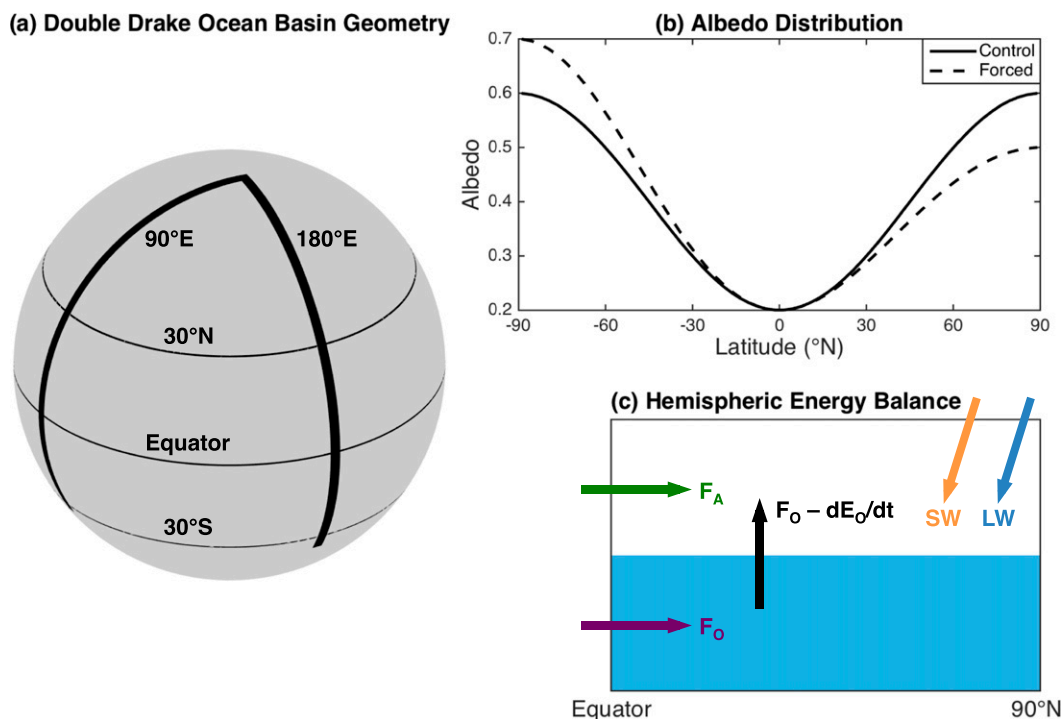
FIG. 2. Model setup and hemispheric energy balance. (a) Ocean basin geometry, showing the two thin ridges at 90°E and 180° extending from 90°N to 35°S, blocking zonal flow in the ocean. (b) Surface albedo distribution for the control (solid) and forced (dashed) model runs. (c) Terms in the hemispheric energy balance corresponding to those in Eq. (2).

model's response to the forcing. In section 3, we analyze the resulting ITCZ shifts in terms of the hemispheric energy balance, showing how cross-equatorial energy transport by the ocean can damp ITCZ shifts. In section 4, we show how the surface wind stress coupling the two fluids results in a wind-driven ocean circulation that always damps ITCZ shifts. In section 5 we describe the characteristics of the anomalous cross-equatorial ocean cell, comparing it to the circulation of the Indian Ocean. A summary and discussion of the results follows in section 6.

2. Model framework and experimental design

We use a coupled atmosphere–ocean version of the MITgcm (Marshall et al. 1997a,b, 2004), run on a cubed-sphere grid with roughly 2.8° horizontal resolution (Adcroft et al. 2004). The atmospheric component of the model has 26 pressure levels and employs a gray radiation scheme as in Frierson (2007). The longwave optical thickness is modified by the distribution of water vapor, following Byrne and O'Gorman (2013), but there are no clouds or shortwave absorption in the atmosphere, and the planetary albedo is equal to the surface albedo. Convection and precipitation are parameterized as in

Frierson (2007), employing a modified Betts–Miller scheme; unstable regions are relaxed to a moist adiabatic lapse rate. A seasonal cycle of insolation at the top of the atmosphere is specified for a circular orbit with a 360-day period, an obliquity of 23.45°, and a solar constant of $1360\,W\,m^{-2}$. We specify a distribution of surface albedo varying from 0.2 at the equator to 0.6 at the poles (Fig. 2b) to broadly mimic the observed distribution of albedo.

To test the impact of the ocean circulation on the ITCZ, we run two configurations of the model: one where the ocean's circulation is "active" and one where it is "passive." The active oceanic component of the model is similar to Enderton and Marshall (2009), with 15 vertical levels spanning a depth of 3.4 km, and parameterizes geostrophic eddies using a Gent–McWilliams/Redi scheme following Griffies et al. (1998). Ocean basins are created by placing infinitesimally wide north–south vertical walls at cell edges, blocking the zonal flow from crossing a line of longitude. Here we use two of these walls, spaced 90° longitude apart and extending from the North Pole to 35°S, to create a two-basin "Double Drake" geometry with a large Southern Ocean (Fig. 2a), as in Ferreira et al. (2010). The fully coupled model with the active ocean is spun up for
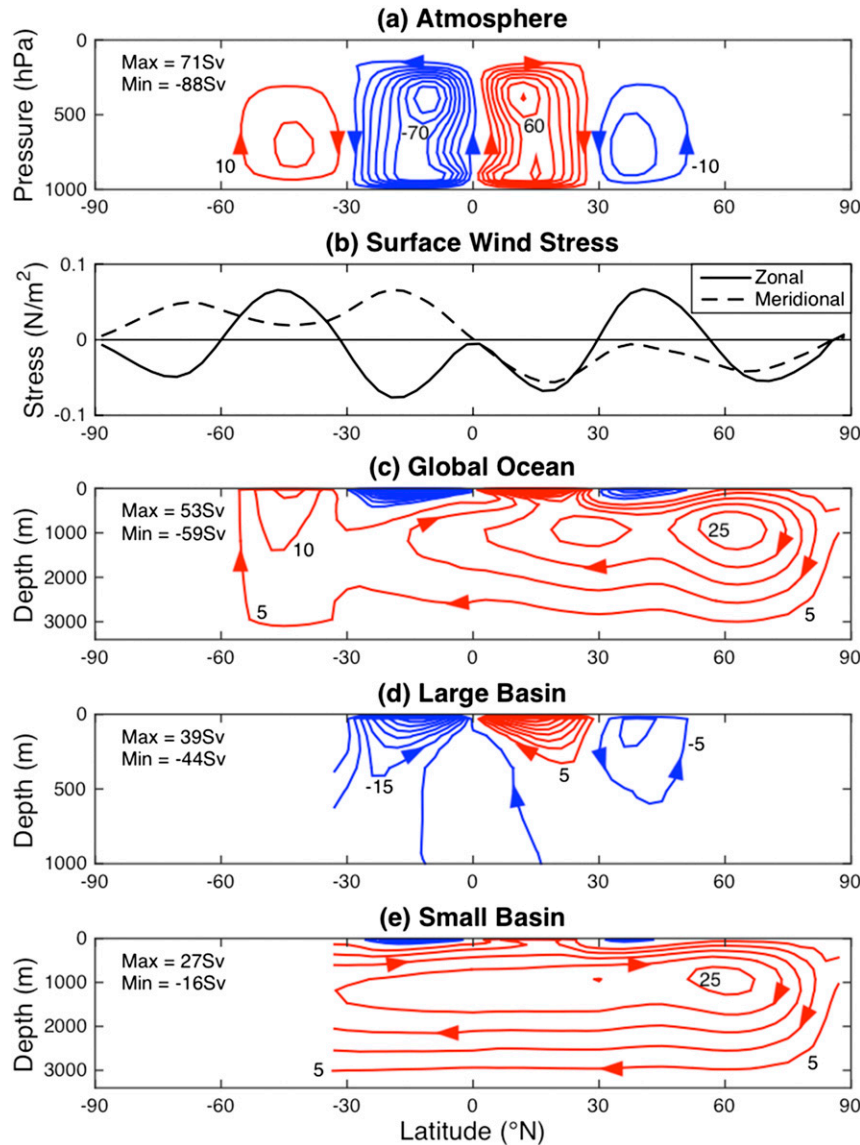
FIG. 3. Fully coupled model run annual mean overturning circulations in the control simulation. (a),(c)–(e) Zonal mean mass transport streamfunctions for the (a) atmosphere (contour interval: 10 Sv), (c) global ocean (contour interval: 5 Sv), and the (d) large and (e) small ocean basins (contour interval: 5 Sv). Red contours indicate positive values and clockwise rotation, and blue contours indicate negative values and counterclockwise rotation, shown by arrows. The zero contour is not shown. (b) Annual mean zonal (solid) and meridional (dashed) surface wind stress on the ocean.

1000 years, at which point there are only small temperature trends in the deep ocean, on the order of 0.1 K century^{-1}.

The atmosphere and ocean circulations in the fully coupled model have features similar to present-day Earth. Hadley cells in the NH and SH extend to roughly 30° latitude (Fig. 3a), and the average of their annual mean strengths is 80 Sv (1 Sv ≡ 10^9 kg s^{-1}), with the NH cell 17 Sv stronger than the SH cell. The surface zonal

wind stress on the ocean (Fig. 3b) is easterly over the width of the Hadley cells and westerly in the extratropics. The 90°-wide small basin has a deep overturning circulation qualitatively similar to the AMOC, while the 270°-wide large basin's circulation is dominated by the shallower subtropical cells and confined to the thermocline, as in the Pacific Ocean (Figs. 3d,e). The global ocean overturning streamfunction between 45° and 60°S shows upwelling in the

(a) Energy Transports
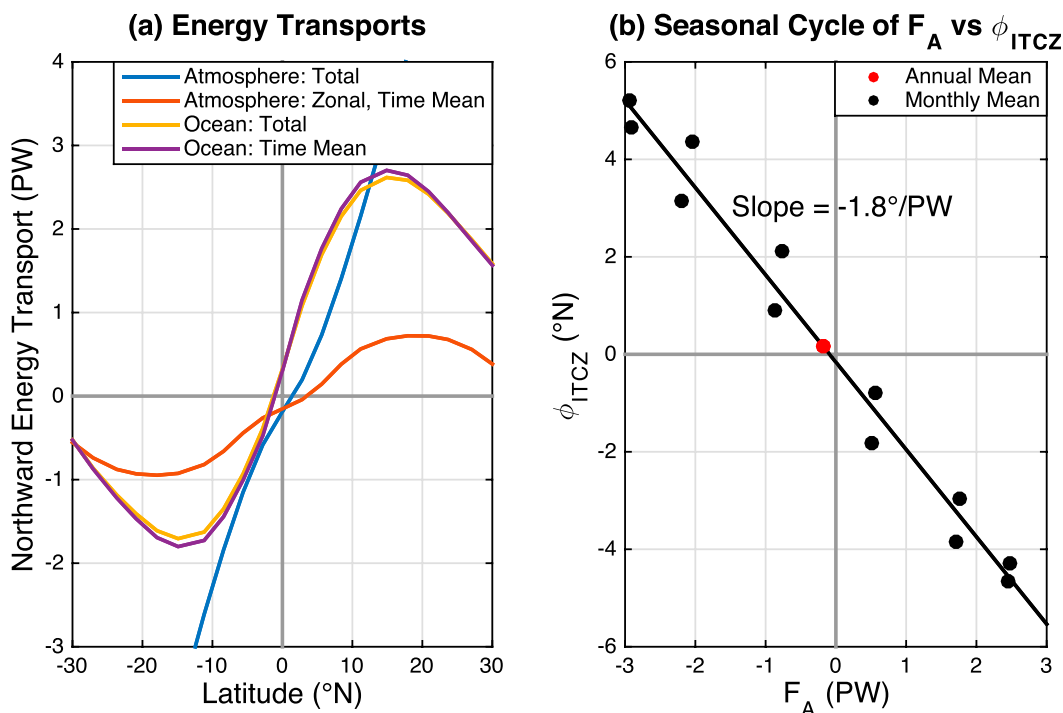

(b) Seasonal Cycle of F_A vs ϕ_{ITCZ}

FIG. 4. Fully coupled model run energy transport climatology. (a) Annual mean northward energy transports in the atmosphere and ocean. (b) Regression of cross-equatorial energy transport by the atmosphere onto the ITCZ position using monthly mean values (black dots) from the control run's seasonal cycle. The red dot is the annual mean ITCZ position and energy transport.

Southern Ocean of deep water formed in the small basin.

Meridional energy transports in the tropics by the atmosphere and ocean are shown in Fig. 4a, with both fluids transporting energy across the equator. The ocean's poleward energy transport is dominated by the time mean circulation, and 0.3 PW of energy is transported northward across the equator as a result of the deep overturning circulation in the small basin. While the time mean, zonal mean Hadley cells in this model accomplish a smaller fraction of the total atmospheric poleward energy transport than in nature (c.f. Marshall et al. 2014, their Fig. 3), they are responsible for nearly all of the atmosphere's 0.2 PW of southward cross-equatorial energy transport. Tied to this southward cross-equatorial energy transport, the ITCZ position—calculated as the centroid of zonal mean precipitation between 20°S and 20°N, following Donohoe et al. (2013)—is in the NH in the annual mean (Fig. 4b). The relationship between the ITCZ position and the atmosphere's cross-equatorial energy transport can also be diagnosed from monthly means over the model's seasonal cycle, and regressing the latter onto the former yields a slope of $1.8° \, \mathrm{PW}^{-1}$ for monthly mean values. This slope is somewhat lower than Earth's $2.7° \, \mathrm{PW}^{-1}$

(Donohoe et al. 2013). One possible reason for this is an excess of total tropical rainfall in our model relative to Earth, making our centroid metric for the ITCZ less sensitive to changes in the tropical rainfall peak. Another is a higher net heating of the atmosphere at the equator in our model relative to Earth, making the position of the ITCZ less sensitive to energetic perturbations in the "energy flux equator" framework of Schneider et al. (2014); see the discussion in the appendix. In the annual mean, the ITCZ resides in the NH, consistent with the stronger SH Hadley cell (Fig. 3a) and southward cross-equatorial energy transport by the atmosphere (Fig. 4a).

Results from "active" ocean model runs are compared to those using a "passive" ocean circulation, which consists of a stationary mixed layer heated by a specified pattern of heat fluxes, often termed a "slab" ocean. These heat fluxes are diagnosed from the annual mean net surface heat flux from the spun-up control run of the fully coupled configuration and represent ocean energy transport convergence into a given grid box. Annual mean mixed layer depths at each grid box are diagnosed from the fully coupled runs and applied as a constant boundary condition. To reduce the spinup time of the model (200 years for the
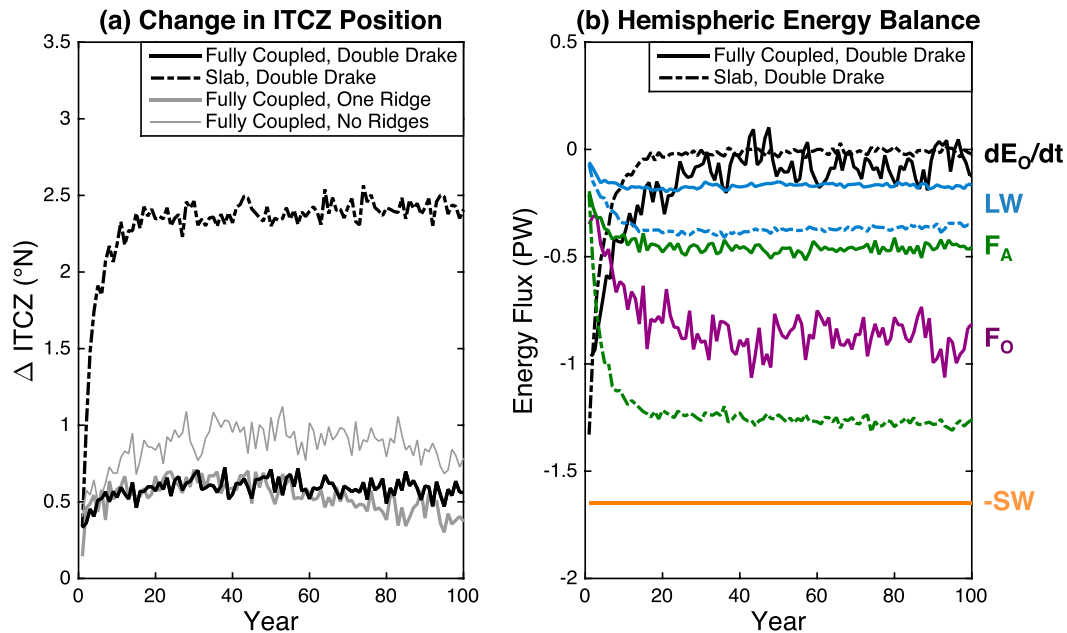
FIG. 5. Composites of ensemble members beginning the year the albedo distribution is changed for the fully coupled (solid) and slab ocean (dashed) model runs. (a) Changes in the latitude of the precipitation centroid. (b) Terms in the Eq. (2) energy budget. Gray lines in (a) indicate ITCZ shifts in fully coupled model runs employing one vertical wall in the ocean at 0° longitude extending from the North Pole to the South Pole (one ridge) or no vertical walls in the ocean to interrupt the flow (no ridges). Note the atmospheric energy tendency in (b) is not plotted, owing to its small magnitude in the annual mean, and that the sign of the shortwave radiation forcing has been reversed.

slab ocean configuration), mixed layer depths are limited to 300 m, only affecting the values near the North Pole in the small basin. The seasonal cycle of mixed layer depths and ocean energy transport in the fully coupled model appear to have a minor impact on the large-scale atmospheric circulation in the tropics: the seasonal cycle of the Hadley cells' strengths and the ITCZ position are similar (respective amplitudes of 199 and 205 Sv for the NH Hadley cell and 9.9° and 10.0° latitude for the fully coupled and slab runs) between the slab ocean and fully coupled cases.

Once both model configurations are spun up, shifts in the ITCZ are forced by modifying the distribution of surface albedo (Fig. 2b), reducing it to 0.5 at the North Pole and increasing it to 0.7 at the South Pole. This has the effect of heating the NH and cooling the SH, and the ITCZ is expected to shift north. Because the atmosphere does not interact with shortwave radiation in our model, all of the resulting heating or cooling initially occurs at the ocean surface. The forcing is applied instantaneously to 10 ensemble members from both the fully coupled and slab ocean models, and ensemble members are initialized with snapshots of fields from their control runs taken at 10-yr intervals. Ensemble means are composited on the year the forcing is applied. Changes in model

fields from the forced runs are differenced from their 300-yr averages in the control runs—years 1001–1300 in the fully coupled model and years 201–500 in the slab ocean model. The adjusted, quasi-equilibrium response to the forcing is taken as the time mean, ensemble mean for years 101–200 after the forcing is applied, during which period trends in the model fields are relatively weak. Since the ocean circulation is free to change in the fully coupled model while its representation in the slab ocean model is fixed, differences in the responses of the two model configurations will serve to highlight the role of an active ocean circulation in affecting the model's response to the albedo forcing.

3. ITCZ shifts and the hemispheric energy balance

Fully coupled runs show a significantly reduced ITCZ shift when compared to runs with a slab ocean. Compositing on the year the albedo distribution is changed, the ITCZ's response to the forcing is weaker at all time scales in the fully coupled runs, and the quasi-equilibrated response shows a reduced shift by a factor of 4.30, from 2.44° in the slab runs to 0.57° (black lines in Fig. 5a). In both the slab and fully coupled runs, the majority of the ITCZ's shift occurs in the first few years

after the albedos are changed. This, when combined with the reduced ITCZ shift in the fully coupled runs during those years, suggests a rapid response of the ocean circulation.

In response to the imposed albedo contrast, the ocean circulation acts to damp the ITCZ shift. This damping can be diagnosed using the hemispheric energy budget, where tendencies of the atmosphere's and ocean's energy content, dE_A/dt and dE_O/dt, respectively, are equal to changes in the incoming fluxes of energy, shown schematically in Fig. 2c. The energy budget for the NH is given by

$$\frac{dE_A}{dt} + \frac{dE_O}{dt} = \text{SW} + \text{LW} + F_A + F_O. \qquad (2)$$

Here the net incoming energy flux is separated into downward shortwave (SW) and longwave (LW) radiation at the top of the atmosphere and northward cross-equatorial energy transports by the atmosphere and ocean (F_A and F_O, respectively). The units in Eq. (2) are watts; tendencies and radiative fluxes are integrated over the hemisphere. The difference between F_O and dE_O/dt is equal to the net flux of energy upward into the atmosphere at the surface. In our analysis, the contribution of the kinetic energy in both fluids to terms in Eq. (2) is neglected, and the energy content of the atmosphere is calculated using the moist enthalpy, equal to the sum of the sensible and latent heats. Energy transport in the atmosphere is calculated as the transport of moist static energy, which is the sum of the moist enthalpy and the potential energy.

After the atmosphere and ocean have adjusted in response to the forcing, in this case SW, the tendency terms go to zero. If the relationship between changes in the ITCZ latitude and the atmosphere's cross-equatorial energy transport is linear, following from Fig. 4b, and given by

$$\Delta\phi_{\text{ITCZ}} = -b\,F_A, \qquad (3a)$$

where b is a positive constant, Eq. (2) can be rearranged to give

$$\Delta\phi_{\text{ITCZ}} = b\,\text{SW}\,C, \qquad (3b)$$

where

$$C = \frac{1}{1 + F_O/F_A + \text{LW}/F_A}. \qquad (3c)$$

Here C is the "degree of compensation" by the atmosphere's cross-equatorial energy transport for the imposed forcing SW. A value of one means SW is perfectly

compensated by F_A and the atmosphere transports the entire heating imbalance across the equator. A value of zero means the atmosphere transports no more energy across the equator, the ocean's cross-equatorial energy transport and longwave radiation compensate SW, and the ITCZ does not move. Diagnosed from values of $\Delta\phi_{\text{ITCZ}}$ and F_A, the constant b is $1.9°\,\text{PW}^{-1}$ for the slab ocean case and $1.3°\,\text{PW}^{-1}$ for the fully coupled case.

Inspecting the terms in Eq. (2) for the slab ocean case, shown by the dashed lines in Fig. 5b, the atmosphere's cross-equatorial energy transport compensates the shortwave forcing much more strongly than increased outgoing longwave radiation. The NH's slab ocean initially absorbs most of the heating imposed by the albedo reduction, but as its energy content tendency decays to zero, the magnitudes of F_A and LW increase to compensate SW. Unless the atmosphere's longwave radiative feedbacks are positive, destabilizing its response to a heating or cooling, LW will have the same sign as F_A, and LW/F_A will be positive. Averaging over years 101–200, the degree of compensation C for the slab ocean runs is 0.79, similar to values seen in previous experiments with a slab ocean and a tropical–subtropical component of the forcing (cf. Seo et al. 2014, their Fig. 3c).

If the ocean circulation is allowed to dynamically adjust, however, the atmosphere is no longer the most strongly compensating component, and cross-equatorial energy transport by the ocean dominates the response in the fully coupled runs (solid lines in Fig. 5b). Because it is deeper, the ocean's energy content tendency takes longer to decay to zero than in the slab ocean runs. Once it does, F_O emerges as the most strongly compensating term followed by F_A then LW. Compared to the slab ocean case, the atmosphere transports less energy across the equator and C decreases to 0.30. The coupled system, however, transports more energy across the equator than the atmosphere does in the slab ocean case. The fraction of the forcing compensated by longwave radiation to space (blue lines) is reduced in the fully coupled runs, where the addition of an active ocean circulation makes the coupled climate system more efficient at compensating the shortwave forcing.

Returning to Eq. (3c), it is clear that cross-equatorial energy transport by the ocean is the largest contributor to the reduced degree of atmospheric compensation in the fully coupled case: LW/F_A is similar for both model configurations (0.27 for the slab ocean and 0.39 for the fully coupled model), but F_O/F_A is 1.98 in the fully coupled case while it is zero in the slab ocean runs. A positive F_O/F_A indicates that the ocean and atmosphere are responding to the albedo forcing by both transporting energy southward across the equator, reducing the fraction of the forcing compensated by the atmosphere in the fully

coupled runs. Put another way, if the ocean is able to partially compensate an imposed heating imbalance, the net imbalance the atmosphere experiences is reduced, and ITCZ shifts are damped when the atmosphere does not have to transport as much energy across the equator.

4. Coupling of the atmosphere and ocean circulations by the surface wind stress

For the ocean to damp ITCZ shifts, it must transport energy across the equator in the same direction as the atmosphere, and the question arises whether that characteristic is robust. It is clear from past modeling studies (see, e.g., Zhang and Delworth 2005; Broccoli et al. 2006) that in some circumstances the opposite can occur. In response to a forced reduction in the strength of the AMOC and its northward energy transport by prescribing a flux of freshwater into the North Atlantic, the atmosphere in those studies shifts the ITCZ southward and transports energy northward across the equator, opposing the ocean's anomalous southward energy transport. However, the shallower STCs are mechanically coupled to the overlying atmosphere through the surface wind stress; their response to forcing will be driven by changes in those winds and could be very different than the AMOC's response to buoyancy forcing in the extratropics. Here we argue that because the STCs are driven by the surface wind stress distribution, they will always transport energy across the equator in the same direction as the atmosphere.

The atmosphere's and ocean's anomalous energy transport in the fully coupled runs are largely achieved by the time mean circulation, which accounts for 69% of the atmosphere's and 100% of the ocean's anomalous cross-equatorial energy transport. Anomalous time mean, zonal mean streamfunctions for the atmosphere and ocean, and zonal mean wind stress anomalies are shown in Fig. 6. Streamfunction anomalies in the atmosphere are stronger than those of the ocean and peak at about 500 hPa. Large-basin ocean mass transport anomalies are strongest in the upper 1000 m, while anomalies in the small basin reflect weakening and shoaling of the deep meridional overturning circulation (MOC). The pattern of zonal wind stress anomalies shows a weakening of the trade winds in the NH and a strengthening in the SH and are consistent with a northward shift of the Hadley cells and the ITCZ. In the extratropics, dipoles of wind stress anomalies reflect a southward shift in the surface westerly jets.

The pattern of zonal wind stress anomalies is asymmetric about the equator, driving southward surface Ekman flow in the tropical ocean in both hemispheres (Fig. 7). South of 12°N, the maximum anomaly in the global ocean's anomalous mass transport streamfunction is equal to the Ekman mass flux times the circumference of a latitude circle, defined as

$$M_{Ek} = 2\pi a \cos\phi \frac{\tau_X}{f}, \qquad (4)$$

where a is the radius of Earth, τ_X is the zonal mean zonal wind stress at the surface, and f is the Coriolis parameter. North of 12°N, changes in the small basin's deep MOC are stronger than the Ekman mass transport anomalies. The deep MOC, with mass transport streamfunction anomalies shown in Fig. 6c peaking at a depth near 2000 m, is not expected to be in Ekman balance with the surface wind stress. When streamfunction anomalies are evaluated near a depth of 150 m, though, they match the Ekman mass transport.

Even though Ekman balance breaks down near the equator, the near linearity of the zonal wind stress anomalies there (Fig. 6b) does not drive strong Ekman suction or pumping, and the surface flow crosses the equator (as in Miyama et al. 2003). The anomalous Ekman mass transports plotted in Fig. 7 are relatively well behaved near the equator because the zonal wind stress anomalies approach zero faster than the Coriolis parameter does. The resulting anomalous cross-equatorial cell (CEC) is seen most clearly in the large basin (Fig. 6d), where Ekman pumping and suction close the circulation at roughly 40°S and 40°N. Southward shifts in the surface westerly jets are responsible for anomalies in extratropical Ekman pumping and suction. The meridional extent of the CEC is set by the distance between the westerly wind maxima in each hemisphere and is significantly larger than the extent of the Hadley cells. While the CEC shares a surface branch with the STCs, it is distinct from them. Comparing Fig. 6d to Fig. 3d, note that the upwelling branch of the STCs is not moved off of the equator and that the return branch of the CEC is deeper than the subsurface flow of the STCs.

Anomalies in the atmosphere's mass transport streamfunction (Fig. 6a) peak in the midtroposphere and are not in Ekman balance with the surface winds equatorward of 15° (Fig. 7). Their vertical structure is similar to the climatological Hadley cells, though—compare Fig. 6a to Fig. 3a—and indicative of a shift in those circulations. Streamfunction anomalies evaluated near the top of the planetary boundary layer at 900 hPa are same-signed as those above and are in Ekman balance with the surface wind stress to within 6° of the equator. This relationship also holds over the seasonal cycle in the control run, indicating that while peak Hadley cell anomalies are not in Ekman balance with the surface zonal wind stress, they are coupled to it.
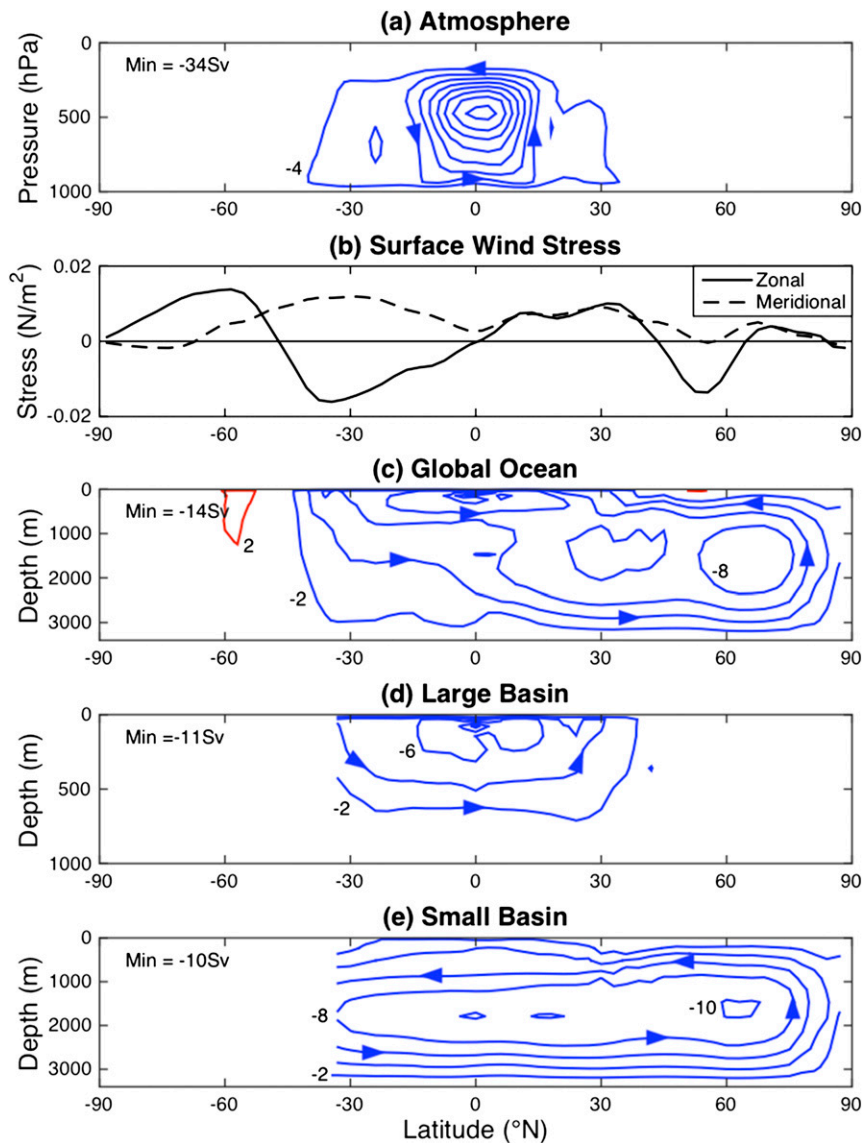
FIG. 6. As in Fig. 3, but for annual mean anomalies in the fully coupled runs, ensemble averaged over years 101–200 after the albedo distribution is changed. (a) Contour interval is 4 Sv. (c)–(e) Contour interval is 2 Sv.

The mass and energy transports of the overturning circulations in both fluids are related by their gross stabilities (Neelin and Held 1987; Held 2001), a measure of the energy contrast between their upper and lower branches. We may write, following Czaja and Marshall (2006) and Held (2001),

$$\frac{F_O}{F_A} = \frac{\psi_O}{\psi_A} \frac{S_O}{S_A}. \tag{5}$$

Gross stabilities S_O and S_A represent the respective energy contrasts between the upper and lower branches of the ocean and atmosphere circulations. Anomalous

energy transports by the atmosphere and ocean are shown in Fig. 7b. As mentioned in section 3, the ocean transports nearly twice as much energy across the equator as the atmosphere, diverging more energy from the NH subtropics and converging it in the SH subtropics. The atmosphere diverges or converges more energy in the extratropical and polar latitudes, primarily through transient eddies and stationary waves rather than the zonal mean, time mean circulation. Near the equator, the atmosphere's southward energy transport decreases, and the zonal mean, time mean Hadley cells are responsible for the majority of the cross-equatorial transport.
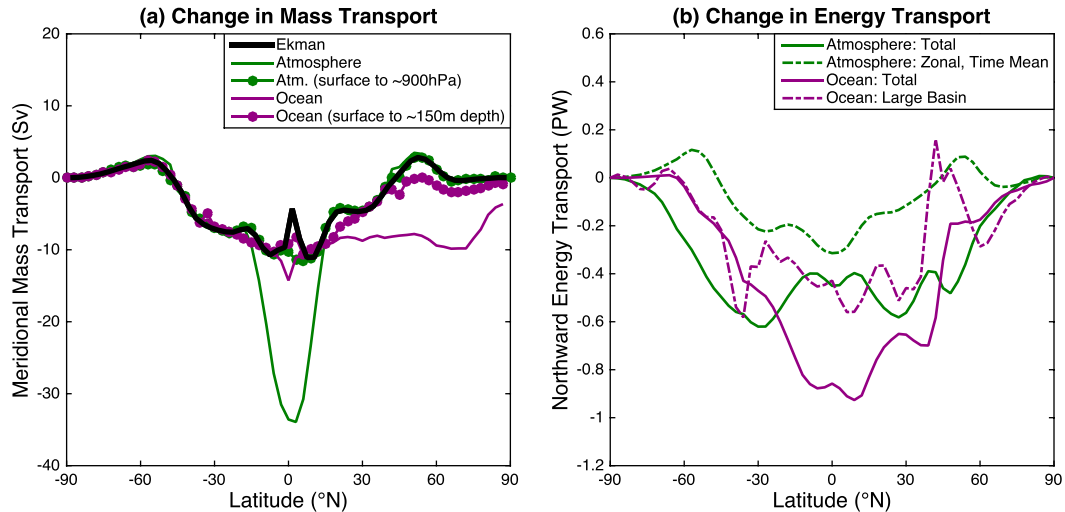
FIG. 7. Mass and energy transport anomalies in the fully coupled model runs. (a) Anomalous Ekman mass transport (black), maximum mass transport streamfunction anomalies at each latitude (solid color), and mass transport streamfunction anomalies in the atmosphere (lines with dots) at the 891-hPa model level (green) and at the 144-m-depth model level in the ocean (purple). (b) Anomalous northward energy transports by the atmosphere and ocean.

Guided by Eq. (5) and dividing anomalous cross-equatorial energy transports by peak mass transport streamfunction anomalies at the equator, the gross stability of the atmosphere is $1.3 \times 10^4 \, \text{J kg}^{-1}$ and the ocean is $6.3 \times 10^4 \, \text{J kg}^{-1}$. The relatively high gross stability in the ocean is expected, since the specific heat capacity of water is larger than that of air, and the tropical thermocline is in general more stratified in temperature than the tropical atmosphere is in moist static energy. So, even though the atmosphere's anomalous circulation is stronger, the ocean transports more energy across the equator. Combining the positive gross stabilities of both fluids with the constraint that their circulations must overturn in the same sense by Ekman balance, making ψ_O/ψ_A positive, F_O/F_A is positive from Eq. (5) and the atmosphere and wind-driven CEC are constrained to transport energy across the equator in the same direction. This coupled cross-equatorial energy transport results in the damping of ITCZ shifts described by Eqs. (3b) and (3c).

5. Large-basin CEC and energy transport

We have shown that the cross-equatorial cell's mass transport is in Ekman balance with the surface wind stress, but its cross-equatorial energy transport is also sensitive to its gross stability, which is set by the properties of the surface and return branches. In this section, we describe the properties and paths of these two branches, how they impact the energy transported by the CEC, and draw comparisons to the annual mean circulation in the Indian Ocean. Our focus will be on the circulation in the large basin, which is responsible for 46% of the ocean's total cross-equatorial energy transport (Fig. 7b). The anomalous circulation in the large basin is shallower and more clearly wind driven than that of the small basin (compare Fig. 6d to Fig. 6e), where changes in the STCs can be difficult to separate from the large changes in the deep MOC.

Transforming the vertical coordinate from depth to temperature, the anomalous mass transport streamfunction in the large basin, including transport by both the steady and unsteady circulation, is shown in Fig. 8. The warmer upper branch roughly follows zonal mean surface conditions, while the denser, colder lower branch conserves temperature as it flows northward across the equator. The temperatures in the lower branch are nearly identical to the seasonal minimum surface temperature—calculated as the average minimum monthly mean surface temperature from the forced runs—at their source latitudes near 40°S, reflecting the Ekman pumping of water caused by the southward shift in the SH westerly jet. The southward cross-equatorial energy transport accomplished by this circulation is 0.41 PW, which when divided by its strength at the equator, 7.2 Sv, gives a gross stability of $5.9 \times 10^4 \, \text{J kg}^{-1}$, close to the value estimated above for the global time mean, zonal mean CEC. Dividing by the specific heat capacity of $3994 \, \text{J kg}^{-1} \, \text{K}^{-1}$ gives a temperature contrast between the upper and lower branches of 14°C, close to the 15°C difference between the −4-Sv contours at the equator in Fig. 8.
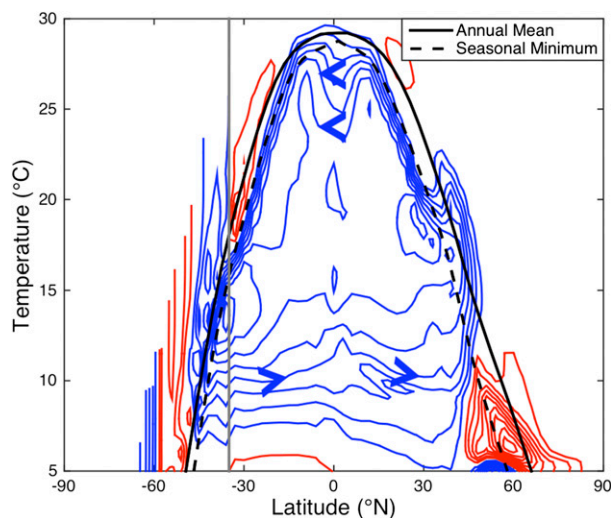
FIG. 8. Mass transport streamfunction anomalies in the large basin, including the contributions from steady and unsteady transport. Contour interval: 1 Sv; the zero contour is not shown. Red contours indicate positive values and clockwise rotation, and blue contours indicate negative values and counterclockwise rotation, shown by chevrons. Black lines indicate zonal mean surface temperature in the large basin from the forced runs in the annual mean (solid) and the minimum monthly mean value calculated from the average seasonal cycle (dashed).

This temperature contrast between the upper and lower branches is set by the SST difference between the tropics and extratropics. Ekman pumping, feeding the return branch of the CEC, is strongest near 40°S where the annual mean SST is 14°C, 15°C cooler than the equator. The water in the return branch is a couple degrees cooler than the annual mean SST at 40°S, though, as it is formed during wintertime. Temperatures in the surface branch at the equator are also a

couple degrees cooler than the annual mean SST there, offsetting the amplitude of the seasonal cycle of SST around 40°S. As a result, the gross stability of the CEC is approximately the annual mean SST difference between the equator and the extratropics, in this case 40°S.

The pathways of the upper and lower branches are shown in Fig. 9, where anomalous currents are displayed at the surface and on the 1026.5 kg m^{-3} potential density surface, a typical value for the lower branch flow. The surface currents forming the upper branch of the CEC diverge near 40°N, cross the equator in the interior of the basin, and converge near 40°S. On the 1026.5 kg m^{-3} potential density surface, water subducted near 40°S travels westward and hits the western boundary at 20°–40°S. The flow then bifurcates; some recirculates southward and the rest travels northward across the equator in a boundary current. This boundary current, integrated over 6°–16°C (corresponding to 240–930-m depth at the equator on the western boundary) and 174°W–180° transports 7.8 Sv, close to the 7.2-Sv strength of the CEC at the equator in Fig. 8.

The anomalous cross-equatorial cell we see in these simulations is reminiscent of the Indian Ocean's shallow overturning circulation. While it has a strong seasonal cycle, the annual mean Indian Ocean CEC is also characterized by cross-equatorial wind-driven flow near the surface and return flow in a deeper western boundary current (Schott et al. 2002), transporting an estimated 0.5 PW of energy southward across the equator (Trenberth and Caron 2001). Annual mean surface zonal wind stress in the Indian Ocean is nearly asymmetric about the equator, and Ekman transports are southward in the interior of the basin at both 3°N and 3°S. Like the anomalous CEC seen in our
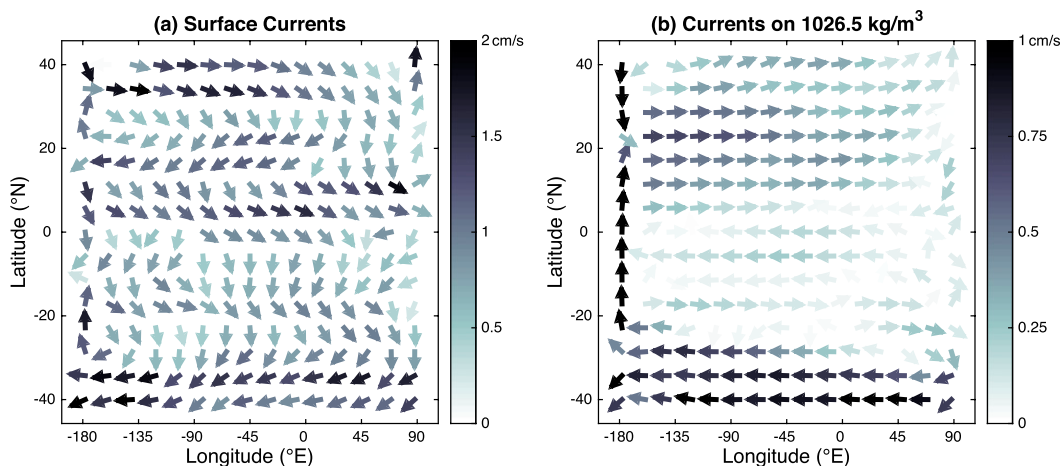

FIG. 9. Pathways of anomalous CEC currents in the large basin. (a) Surface branch. (b) Return branch. Current speed is shown by shading, and direction is shown by arrows.

simulations, the annual mean Indian Ocean CEC returns this cross-equatorial mass transport in a deeper western boundary current, the Somali current, whose water eventually upwells in the NH.

The Indian Ocean, however, has a counterrotating "equatorial roll" under which the surface Ekman currents pass to cross the equator. The equatorial roll in observations is 50–100 m deep and only ~2° latitude wide, too narrow to be simulated in our model, and is not seen in Fig. 6d. We do, however, notice near the equator a weakening of surface currents in Fig. 9a and a dip to temperatures lower than zonal mean surface values of the surface branch in Fig. 8. Near the equator, the surface branch is confined to the first model level, but in the grid cells immediately surrounding the equator, the southward flow spreads to the second model level (not shown) and slightly cooler temperatures. Because of its shallow depth, the Indian Ocean equatorial roll resides mostly in the weakly stratified mixed layer and does not significantly contribute to cross-equatorial energy transport in the Indian Ocean (Schott et al. 2002; Miyama et al. 2003). From the perspective of its cross-equatorial energy transport, then, the Indian Ocean CEC is an analog of our anomalous CEC, with warm water moving southward near the surface and cooler water subducted by Ekman pumping returning northward in a western boundary current in the thermocline.

6. Summary and discussion

By forcing a coupled ocean–atmosphere model with an interhemispheric albedo contrast and allowing the ocean circulation to adjust, we find that the resulting ITCZ shift is damped by a factor of 4 compared to a configuration where the ocean circulation is held fixed. The adjusted ocean circulation transports energy from the heated hemisphere to the cooled one, and its resulting cross-equatorial energy transport is the largest term in the atmosphere's adjusted hemispheric energy balance, helping offset the heating contrast imposed by the albedo distribution. As a result, the atmosphere is not required to transport as much energy across the equator than if the ocean circulation is held fixed. It therefore does not compensate the heating contrast as strongly as when coupled to a slab ocean, and so the magnitude of the ITCZ shift is reduced. Key to this reduction is the anomalous ocean circulation acting to transport energy across the equator in the same direction as the atmosphere, reducing the atmosphere's hemispheric heating imbalance.

We argue that the mechanical coupling between the Hadley cells, surface wind stress, and the tropical–subtropical ocean circulation ensures that that ocean circulation always acts to transport energy across the equator in the same direction as the atmosphere. This is accomplished by an Ekman-driven CEC. The strength of the CEC is set by interhemispheric asymmetries in the trade winds. Its energy contrast is determined by the SST difference between the tropics and the extratropics, where the shift in the surface westerly jet sets the temperature of the subducted water forming its lower branch. By acting on a larger energy contrast than the Hadley cells, the CEC is more efficient at transporting energy across the equator than the atmosphere, and it transports more energy across the equator even though it is a weaker circulation.

The CEC is a hemispherically asymmetric circulation and thus can be separated from the symmetric STCs by decomposing the mass transport streamfunction into symmetric and asymmetric components as in Fig. 1. This decomposition ensures that the symmetric circulation, shown schematically in Fig. 1b, is largely responsible for energy transport out of the tropics to higher latitudes but not across the equator since its strength goes to zero there. The hemispherically asymmetric circulation in Fig. 1c then represents the component that transports energy across the equator, enabling the ocean to compensate for interhemispheric heating asymmetries. Comparing Fig. 1b to Fig. 1c, the hemispherically asymmetric CEC extends deeper than the symmetric STCs and transports energy southward across the equator owing to its positive gross stability. The deeper CEC, whose lower branch water is subducted in the cooler extratropics, wraps around the shallower STCs, whose lower branch waters are subducted in the warmer subtropics.

The CEC in our simulations has characteristics reminiscent of the annual mean Indian Ocean circulation, with its surface branch crossing the equator in the interior of the basin and its lower branch crossing the equator in a western boundary current. Returning to Fig. 5, though, the details of ocean basin geometry and the pathway of the lower branch appear to have a secondary effect. The two solid gray lines show ITCZ shifts from fully coupled simulations where, instead of a Double Drake ocean basin geometry, the model's ocean has either a single vertical wall (one ridge) extending from the North Pole to the South Pole or no walls at all (no ridges). In all three cases, the ITCZ shift is significantly reduced as compared to slab ocean runs, even when no western boundary current can form as in the no-wall case. The ITCZ shift time scale changes with ocean basin geometry, and its amplitude varies by a couple tenths of a degree across the cases, but the consistent damping of the shift by a fully coupled ocean

circulation suggests the details of the ocean basin geometry are unimportant to leading order.

We believe that our key result—the ocean acting to damp ITCZ shifts—is insensitive to the choice of forcing, owing to the mechanical coupling of the atmosphere and ocean circulations by the surface wind stress. For example, if a large freshwater pulse floods an ocean basin containing a deep overturning circulation such as the AMOC, reducing its strength and northward energy transport as in Zhang and Delworth (2005), we can expect the resulting ITCZ shift to induce a wind-driven CEC that transports energy northward across the equator in the same sense as the overlying atmosphere. The CEC's northward energy transport would then oppose the deep circulation's anomalous southward energy transport, offsetting a large fraction of the interhemispheric heating experienced by the atmosphere, damping the ITCZ shift. Furthermore, our results are not affected by the slope of the ITCZ position–atmospheric cross-equatorial energy transport relationship. While our model's slope of $-1.8° \, \mathrm{PW}^{-1}$ (Fig. 4b) is shallower than it is for Earth, the factor-of-4 damping of ITCZ shifts by the ocean circulation is insensitive to the slope because it reflects the relative magnitudes of the shifts, not their absolute values (see the appendix).

Damping of ITCZ shifts by a wind-driven CEC may help explain some of the recent results seen in more comprehensive coupled atmosphere–ocean GCMs. In both Kay et al. (2016) and Tomas et al. (2016), ITCZ shifts are strongly damped in fully coupled models compared to slab ocean models, and anomalous cross-equatorial energy transport is dominated by the ocean in those papers and in Hawcroft et al. (2016). The hemispherically asymmetric pattern of trade wind anomalies in the Pacific in Tomas et al. (2016, their Fig. 6a) would drive a southward cross-equatorial surface flow, constituting the surface branch of a CEC as described here. Isolating the asymmetric streamfunction anomalies would help identify if such circulation exists in their model. In Kay et al. (2016), the trade winds in the SH strengthen in all basins relative to the NH, and their hemispherically asymmetric component would drive a CEC in the thermocline hinted at in their Fig. 10. Perhaps the clearest indication of a wind-driven CEC in a fully coupled GCM can be seen in Hawcroft et al. (2016, their Fig. 7), where changes in the cross-equatorial energy transport by the ocean are dominated by the Pacific Ocean, which does not have a deep overturning circulation like the Atlantic. Combined with the relative increase of the trade winds in the SH (Hawcroft et al. 2016, their Figs. 3b–e), their results strongly hint at a large cross-equatorial energy transport (0.2–0.3 PW) by a wind-driven CEC.

Of course, our model simulations are for an idealized, water-covered planet, and several differences between our model configuration and Earth would likely have some impact on the efficacy of the CEC to compensate an interhemispheric heating contrast. Aside from the obvious reduction in surface area covered by the ocean, a significant fraction of Earth's annual mean cross-equatorial mass transport associated with the Hadley cell occurs in the Somali jet (Heaviside and Czaja 2013). The wind stress resulting from such a concentrated atmospheric current might not drive the kind of oceanic CEC we see here. Additionally, the gross stability of the CEC in our simulations is set by Ekman pumping in the SH extratropics resulting from a southward shift in the surface westerly jet. If a different choice of forcing results in no shift of the surface westerly jet, the gross stability of the CEC would be reduced because its lower branch would be supplied by warmer water subducted in the subtropics. The CEC would then transport less energy across the equator, reducing its capacity to compensate the heating contrast and damp the ITCZ shift.

In summary, our results indicate that the ITCZ's position might be far less sensitive to interhemispheric heating contrasts than previously thought and that the wind-driven ocean circulation can strongly compensate for such forcings. As an example, Earth's ITCZ position and atmospheric cross-equatorial energy transport are related by a slope of roughly $2.7° \, \mathrm{PW}^{-1}$ (Donohoe et al. 2013). For a degree of compensation of 80%—appropriate if the ocean circulation is held fixed and F_O is set to zero in Eq. (3c)—the ITCZ would shift by 5° for 2.3 PW of forcing [Eq. (3b)]. If the ocean's cross-equatorial energy transport is not fixed and this sensitivity is reduced by a factor of 4 as a consequence of that transport, then a forcing of 9.1 PW is required to induce the same 5° ITCZ shift. This is equivalent to a massive $36 \, \mathrm{W \, m}^{-2}$ heating over an entire hemisphere. In other words, to induce a northward ITCZ shift of 5°, the SH's mean albedo would have to be increased by roughly 0.1, equivalent to covering an otherwise bare ocean surface with sea ice poleward of 30°S. Such a back-of-the-envelope calculation almost certainly overestimates the forcing necessary to realize a 5° ITCZ shift, it but serves to highlight the dramatic changes in hemisphere mean climate necessary to move the global ITCZ more than a couple degrees off of the equator.

Aaron Donohoe and comments by three anonymous reviewers are gratefully acknowledged.

APPENDIX

ITCZ Shifts in the Energy Flux Equator Framework

The "energy flux equator" framework proposed in Bischoff and Schneider (2014) and Schneider et al. (2014) is similar to but distinct from the approach of Donohoe et al. (2013) and that taken in our Eq. (3). Rather than relating the location of the precipitation centroid to the atmosphere's cross-equatorial energy transport by a constant regression coefficient, as in Eq. (3a), it defines the ITCZ position as the location where the atmosphere's meridional energy transport goes to zero. Despite these differences, though, the energy flux equator framework is useful in understanding why the slope of the relationship between the ITCZ position and the atmosphere's cross-equatorial energy transport in Fig. 4b ($-1.8°\,\mathrm{PW}^{-1}$) is shallower than in the observations ($-2.7°\,\mathrm{PW}^{-1}$; Donohoe et al. 2013). Equation (2) in Schneider et al. (2014) estimates the ITCZ position δ as

$$\delta \approx -\frac{1}{a}\frac{F_0}{S_0 - L_0 - O_0}, \qquad (A1)$$

where a is the radius of Earth, F_0 is the cross-equatorial energy transport by the atmosphere, S_0 is the net downward shortwave radiation at the top of the atmosphere, L_0 is the outgoing longwave radiation at the top of the atmosphere, and O_0 is the downward flux of energy at the ocean surface, which, in a steady state, represents ocean heat transport divergence. The subscript 0 denotes values taken at the equator.

The slope of the ITCZ–atmospheric energy transport relationship can be found by dividing Eq. (A1) by F_0:

$$\frac{\delta}{F_0} = -\frac{1}{2\pi a^2}\frac{1}{\mathrm{NEI}}, \qquad (A2a)$$

where

$$\mathrm{NEI} = \frac{1}{2\pi a}(S_0 - L_0 - O_0) \qquad (A2b)$$

is the net energy input into the atmosphere at the equator ($\mathrm{W\,m^{-2}}$). Using the $32\,\mathrm{W\,m^{-2}}$ diagnosed from our simulations and the $18\,\mathrm{W\,m^{-2}}$ assumed by Schneider et al. (2014), the slopes are $-7°$ and $-13°\,\mathrm{PW}^{-1}$ respectively. It is worth noting that the $-7°\,\mathrm{PW}^{-1}$ slope using the energy flux equator metric is much higher than the $-1.8°\,\mathrm{PW}^{-1}$ using the precipitation centroid metric and that NEI is nearly identical (within $0.4\,\mathrm{W\,m^{-2}}$) between the slab runs

and the fully coupled runs by design. One way to increase the steepness of the slope, bringing it closer to the observations, would be to increase the albedo at the equator. This would decrease S_0, and likely L_0, and thus NEI.

However, NEI (and hence equatorial albedo) plays a negligible role when considering the relative ITCZ shifts in slab ocean and fully coupled model runs. We can see this as follows. Starting from Eqs. (A1) and (A2b), a change in the ITCZ position $\Delta\delta$ is expressed as

$$\Delta\delta = -\frac{1}{2\pi a^2}\Delta\left(\frac{F_0}{\mathrm{NEI}}\right) \qquad (A3a)$$

$$= -\frac{1}{2\pi a^2}\frac{1}{\mathrm{NEI}}\left(\Delta F_0 - F_0\frac{\Delta \mathrm{NEI}}{\mathrm{NEI}}\right). \qquad (A3b)$$

Inspecting the terms in Eq. (A3b), ΔF_0 is at least one order of magnitude larger than the other term in both the slab ocean and fully coupled model runs. This makes intuitive sense given the nature of the interhemispheric forcing: the albedo at the equator is not changed (S_0 is unchanged), the temperature there does not significantly change (L_0 changes are small), and the ocean is transporting energy across the equator, not converging or diverging it there (O_0 changes are small). In this limit, the fractional change in NEI is small and the ITCZ shift can be expressed as follows:

$$\Delta\delta \approx -\frac{1}{2\pi a^2}\frac{\Delta F_0}{\mathrm{NEI}}. \qquad (A4)$$

The ratio of the ITCZ shift in the slab ocean case (subscript slab) to the fully coupled case (subscript cpl) is then the ratio of the anomalous cross-equatorial energy transports:

$$\frac{\Delta\delta_{\mathrm{slab}}}{\Delta\delta_{\mathrm{cpl}}} = \frac{(\Delta F_0)_{\mathrm{slab}}}{(\Delta F_0)_{\mathrm{cpl}}}, \qquad (A5)$$

and NEI plays no role. Using Eq. (A5), the ratio of the ITCZ shifts is 2.87, nearly identical to the 2.81 estimated using shifts calculated from Eq. (A3b), which makes no assumptions about changes in the equatorial energy balance. It is worth noting that these ratios are lower than the value of 4 we use in our paper because of the metric used to calculate the ITCZ shift (precipitation centroid vs energy flux equator), not the model setup.

REFERENCES

Adam, O., T. Bischoff, and T. Schneider, 2016: Seasonal and interannual variations of the energy flux equator and ITCZ. Part I: Zonally averaged ITCZ position. *J. Climate*, **29**, 3219–3230, doi:10.1175/JCLI-D-15-0512.1.

Adcroft, A., J. M. Campin, C. Hill, and J. Marshall, 2004: Implementation of an atmosphere–ocean general circulation

model on the expanded spherical cube. *Mon. Wea. Rev.*, **132**, 2845–2863, doi:10.1175/MWR2823.1.

Bischoff, T., and T. Schneider, 2014: Energetic constraints on the position of the intertropical convergence zone. *J. Climate*, **27**, 4937–4951, doi:10.1175/JCLI-D-13-00650.1.

Broccoli, A. J., K. A. Dahl, and R. J. Stouffer, 2006: Response of the ITCZ to Northern Hemisphere cooling. *Geophys. Res. Lett.*, **33**, L01702, doi:10.1029/2005GL024546.

Byrne, M. P., and P. A. O'Gorman, 2013: Land–ocean warming contrast over a wide range of climates: Convective quasi-equilibrium theory and idealized simulations. *J. Climate*, **26**, 4000–4016, doi:10.1175/JCLI-D-12-00262.1.

Charney, J. G., 1963: A note on large-scale motions in the tropics. *J. Atmos. Sci.*, **20**, 607–609, doi:10.1175/1520-0469(1963)020<0607: ANOLSM>2.0.CO;2.

Chiang, J. C., and C. M. Bitz, 2005: Influence of high latitude ice cover on the marine intertropical convergence zone. *Climate Dyn.*, **25**, 477–496, doi:10.1007/s00382-005-0040-5.

Czaja, A., and J. Marshall, 2006: The partitioning of poleward heat transport between the atmosphere and ocean. *J. Atmos. Sci.*, **63**, 1498–1511, doi:10.1175/JAS3695.1.

Donohoe, A., J. Marshall, D. Ferreira, and D. McGee, 2013: The relationship between ITCZ location and cross-equatorial atmospheric heat transport: From the seasonal cycle to the last glacial maximum. *J. Climate*, **26**, 3597–3618, doi:10.1175/JCLI-D-12-00467.1.

——, ——, ——, K. Armour, and D. McGee, 2014: The interannual variability of tropical precipitation and interhemispheric energy transport. *J. Climate*, **27**, 3377–3392, doi:10.1175/JCLI-D-13-00499.1.

Emanuel, K. A., J. D. Neelin, and C. S. Bretherton, 1994: On large-scale circulations in convecting atmospheres. *Quart. J. Roy. Meteor. Soc.*, **120**, 1111–1143, doi:10.1002/qj.49712051902.

Enderton, D., and J. Marshall, 2009: Explorations of atmosphere–ocean–ice climates on an aquaplanet and their meridional energy transports. *J. Atmos. Sci.*, **66**, 1593–1611, doi:10.1175/2008JAS2680.1.

Ferreira, D., J. Marshall, and J. M. Campin, 2010: Localization of deep water formation: Role of atmospheric moisture transport and geometrical constraints on ocean circulation. *J. Climate*, **23**, 1456–1476, doi:10.1175/2009JCLI3197.1.

Frierson, D. M. W., 2007: The dynamics of idealized convection schemes and their effect on the zonally averaged tropical circulation. *J. Atmos. Sci.*, **64**, 1959–1976, doi:10.1175/JAS3935.1.

——, and Coauthors, 2013: Contribution of ocean overturning circulation to tropical rainfall peak in the Northern Hemisphere. *Nat. Geosci.*, **6**, 940–944, doi:10.1038/ngeo1987.

Griffies, S. M., A. Gnanadesikan, R. C. Pacanowski, V. D. Larichev, J. K. Dukowicz, and R. D. Smith, 1998: Isoneutral diffusion in a *z*-coordinate ocean model. *J. Phys. Oceanogr.*, **28**, 805–830, doi:10.1175/1520-0485(1998)028<0805: IDIAZC>2.0.CO;2.

Hawcroft, M., J. M. Haywood, M. Collins, A. Jones, A. C. Jones, and G. Stephens, 2016: Southern Ocean albedo, inter-hemispheric energy transports and the double ITCZ: global impacts of biases in a coupled model. *Climate Dyn.*, **48**, 2279–2295, doi:10.1007/s00382-016-3205-5.

Heaviside, C., and A. Czaja, 2013: Deconstructing the Hadley cell heat transport. *Quart. J. Roy. Meteor. Soc.*, **139**, 2181–2189, doi:10.1002/qj.2085.

Held, I. M., 2001: The partitioning of the poleward energy transport between the tropical ocean and atmosphere. *J. Atmos.*

Sci., **58**, 943–948, doi:10.1175/1520-0469(2001)058<0943: TPOTPE>2.0.CO;2.

Hwang, Y.-T., and D. M. W. Frierson, 2013: Link between the double-intertropical convergence zone problem and cloud biases over the Southern Ocean. *Proc. Natl. Acad. Sci. USA*, **110**, 4935–4940, doi:10.1073/pnas.1213302110.

Jayne, S. R., and J. Marotzke, 2001: The dynamics of ocean heat transport variability. *Rev. Geophys.*, **39**, 385–411, doi:10.1029/2000RG000084.

Kang, S. M., I. M. Held, D. M. W. Frierson, and M. Zhao, 2008: The response of the ITCZ to extratropical thermal forcing: Idealized slab-ocean experiments with a GCM. *J. Climate*, **21**, 3521–3532, doi:10.1175/2007JCLI2146.1.

Kay, J. E., C. Wall, V. Yettella, B. Medeiros, C. Hannay, P. Caldwell, and C. Bitz, 2016: Global climate impacts of fixing the Southern Ocean shortwave radiation bias in the Community Earth System Model (CESM). *J. Climate*, **29**, 4617–4636, doi:10.1175/JCLI-D-15-0358.1.

Klinger, B. A., and J. Marotzke, 2000: Meridional heat transport by the subtropical cell. *J. Phys. Oceanogr.*, **30**, 696–705, doi:10.1175/1520-0485(2000)030<0696:MHTBTS>2.0.CO;2.

Lindzen, R. S., and A. V. Hou, 1988: Hadley circulations for zonally averaged heating centered off the equator. *J. Atmos. Sci.*, **45**, 2416–2427, doi:10.1175/1520-0469(1988)045<2416: HCFZAH>2.0.CO;2.

Marshall, J., A. Adcroft, C. Hill, L. Perelman, and C. Heisey, 1997a: A finite-volume, incompressible Navier Stokes model for studies of the ocean on parallel computers. *J. Geophys. Res.*, **102**, 5753–5766, doi:10.1029/96JC02775.

——, C. Hill, L. Perelman, and A. Adcroft, 1997b: Hydrostatic, quasi-hydrostatic, and nonhydrostatic ocean modeling. *J. Geophys. Res.*, **102**, 5733–5752, doi:10.1029/96JC02776.

——, A. Adcroft, J. M. Campin, C. Hill, and A. White, 2004: Atmosphere–ocean modeling exploiting fluid isomorphisms. *Mon. Wea. Rev.*, **132**, 2882–2894, doi:10.1175/MWR2835.1.

——, A. Donohoe, D. Ferreira, and D. McGee, 2014: The ocean's role in setting the mean position of the inter-tropical convergence zone. *Climate Dyn.*, **42**, 1967–1979, doi:10.1007/s00382-013-1767-z.

McCreary, J. P., Jr., and P. Lu, 1994: Interaction between the subtropical and equatorial ocean circulations: The subtropical cell. *J. Phys. Oceanogr.*, **24**, 466–497, doi:10.1175/1520-0485 (1994)024<0466:IBTSAE>2.0.CO;2.

Mechoso, C. R., and Coauthors, 2016: Can reducing the incoming energy flux over the Southern Ocean in a CGCM improve its simulation of tropical climate? *Geophys. Res. Lett.*, **43**, 11 057–11 063, doi:10.1002/2016GL071150.

Miyama, T., J. P. McCreary Jr., T. G. Jensen, J. Loschnigg, S. Godfrey, and A. Ishida, 2003: Structure and dynamics of the Indian-Ocean cross-equatorial cell. *Deep-Sea Res. II*, **50**, 2023–2047, doi:10.1016/S0967-0645(03)00044-4.

Neelin, J. D., 1997: Implications of convective quasi-equilibrium for the large-scale flow. *The Physics and Parameterization of Moist Atmospheric Convection*, R. K. Smith, Ed., Springer, 413–446.

——, and I. M. Held, 1987: Modeling tropical convergence based on the moist static energy budget. *Mon. Wea. Rev.*, **115**, 3–12, doi:10.1175/1520-0493(1987)115<0003: MTCBOT>2.0.CO;2.

Schneider, T., T. Bischoff, and G. H. Haug, 2014: Migrations and dynamics of the intertropical convergence zone. *Nature*, **513**, 45–53, doi:10.1038/nature13636.

Schott, F. A., M. Dengler, and R. Schoenefeldt, 2002: The shallow overturning circulation of the Indian Ocean. *Prog. Oceanogr.*, **53**, 57–103, doi:10.1016/S0079-6611(02)00039-3.

Seo, J., S. M. Kang, and D. M. W. Frierson, 2014: Sensitivity of intertropical convergence zone movement to the latitudinal position of thermal forcing. *J. Climate*, **27**, 3035–3042, doi:10.1175/JCLI-D-13-00691.1.

Tomas, R. A., C. Deser, and L. Sun, 2016: The role of ocean heat transport in the global climate response to projected Arctic sea ice loss. *J. Climate*, **29**, 6841–6859, doi:10.1175/JCLI-D-15-0651.1.

Trenberth, K. E., and J. M. Caron, 2001: Estimates of meridional atmosphere and ocean heat transports. *J. Climate*, **14**, 3433–3443, doi:10.1175/1520-0442(2001)014<3433:EOMAAO>2.0.CO;2.

Voigt, A., B. Stevens, J. Bader, and T. Mauritsen, 2014: Compensation of hemispheric albedo asymmetries by shifts of the ITCZ and tropical clouds. *J. Climate*, **27**, 1029–1045, doi:10.1175/JCLI-D-13-00205.1.

Zhang, R., and T. L. Delworth, 2005: Simulated tropical response to a substantial weakening of the Atlantic thermohaline circulation. *J. Climate*, **18**, 1853–1860, doi:10.1175/JCLI3460.1.